Shape from Shading Based on Lax-Friedrichs Fast Sweeping and Regularization Techniques With Applications to Document Image Restoration

Li Zhang† Andy M. Yip‡ Chew Lim Tan†
† School of Computing, 3 Science Drive 2, National University of Singapore
{zhangli,tancl}@comp.nus.edu.sg
‡ Department of Mathematics, 2 Science Drive 2, National University of Singapore
andyyip@nus.edu.sg

Abstract

In this paper, we describe a 2-pass iterative scheme to solve the general partial differential equation (PDE) related to the Shape-from-Shading (SFS) problem under both distant and close point light sources. In particular, we discuss its applications in restoring warped document images that often appear in the daily snapshots. The proposed method consists of two steps. First the image irradiance equation is formulated as a static Hamilton-Jacobi (HJ) equation and solved using a fast sweeping strategy with Lax-Friedrichs Hamiltonian. However, abrupt errors may arise when applying to real document images due to noises in the approximated shading image. To reduce the noise sensitivity, a minimization method thus follows to smooth out the abrupt ridges in the initial result and produce a better reconstruction. Experiments on synthetic surfaces show promising results comparing to the ground truth data. Moreover, a general framework is developed, which demonstrates that the SFS method can help to remove both geometric and photometric distortions in warped document images for better visual appearance and higher recognition rate.

1. Introduction

Shape recovery is a classic and fundamental problem in computer vision. Its goal is to derive a 3D scene description from one or more 2D images. Over the years, researchers have developed a variety of techniques to tackle this problem known as Shape-from-X where X can be shading, stereo, motion, texture, etc. In particular, Shape-from-Shading tries to make use of the shading variations in a single 2D image to reconstruct the original surface shape. The research in this field was pioneered by Horn who first formulated the SFS problem as that of finding the solution of a nonlinear first-order PDE called the brightness equation [12]. Following this, a series of variational methods [14, 13, 11] are developed which try to minimize an energy function that often comprises of an integral of the brightness error to find the solution. Later Oliensis and Dupuis propose to cast the SFS problem as an optimal control problem and directly find the depth map of the surfaces [18]. This brought out a new set of propagation approaches based on the theory of viscosity solutions to Hamilton-Jacobi equations [24, 22, 21]. According to the numerical schemes used to estimate the viscosity solutions, these methods can be further divided into two categories. The first class of methods are based on the monotonicity of the solution along the characteristic direction. Examples are the level set method [19, 16] and the fast marching method [25] proposed by Sethian. In the fast marching method, the solutions are found by using Dijkstra algorithm with a dynamic programming strategy. The time complexity of such a method is $O(NlogN)$, where N is the total number of grid points. Various adaptations of the fast marching method have been developed to handle oblique light source [17] and perspective projection [28, 32]. However, most of them assume the Hamiltonian is convex and homogeneous. Recently, Prados and Soatto extend the fast marching method to handle situations in which the solution is not systematically decreasing along the optimal trajectories [23] with results on some synthetic images. On the other hand, the second class of methods make use of iteration strategies. Rouy and Tourin exploit an upwind and monotone scheme to solve the discretized Eikonal equation iteratively and the convergence property is shown [24]. Tsai *et al.* combine the upwind monotone Godunov Hamiltonian with a Gauss-Seidel iteration method to reconstruct surfaces with good efficiency [31]. Besides the variational methods and propagation methods, linear approaches and local approaches are also developed. Linear approaches compute the solution by performing certain linearization to the reflectance map [30]. Local approaches derive the surface shapes based on the assumption of certain surface type such as spherical surface

1-4244-1180-7/07/$25.00 ©2007 IEEE

[20]. More comprehensive surveys can be found in [33, 9].

In this paper, we focus on the SFS problem under the assumption of perspective projection with both distant and close point light sources. Studying close point light source makes the SFS problem more applicable to real situations in which an image is captured with the on-camera flash. In both cases, the image irradiance equation can be formulated as a static HJ equation with slightly different forms and parameters. To solve the HJ equation, we first use a fast sweeping iterative scheme based on Lax-Friedrichs Hamiltonian to obtain an initial estimate of the surface height. Next, we further improve the shape by minimizing the total brightness error with a regularization term to control the smoothness of the surface. This is necessary because the first step is sensitive to noise and often produces results with abrupt errors when the shading is imperfect. On the other hand, using the result returned from the first step as an initial approximation for the minimization method helps to avoid the problem of being trapped at local minima. Experiments on various synthetic surfaces show promising results comparing to the ground truth data as well as the results from existing approaches. As an application to document image restoration (DIR), we also describe a general framework that illustrates how the SFS method can be used to remove both geometric and photometric distortions in warped document images. Results on real images of different surface shapes are shown and discussed. This further demonstrates that SFS can be applied to real applications as reported in some earlier literature [22, 7].

2. SFS Formulation

To ensure that unambiguous geometrical properties of an object can be inferred from the image irradiance, some assumptions need to be imposed on the SFS formulation. One important common assumption made in most of the approaches is a known reflectance map. A reflectance map specifies the radiance of the surface as a function of its orientation. In particular, the reflectance map for a Lambertian surface under a distant point light source is defined as:

$$I(u,v) = N \cdot L = \frac{(-p,-q,1)}{\sqrt{p^2+q^2+1}} \cdot \frac{(\alpha,\beta,\gamma)}{\sqrt{\alpha^2+\beta^2+\gamma^2}} \quad (1)$$

where $I(u,v)$ is the image irradiance at the image point (u,v) corresponding to the surface point (x,y), (α,β,γ) is the illumination direction and $(-p,-q,1)$ is the surface normal at point (x,y). Let $z(u,v)$ denote the distance from the surface point (x,y) to the u-v plane, then we have the surface gradients: $p = \frac{\partial z}{\partial u}$ and $q = \frac{\partial z}{\partial v}$. This is the general image irradiance equation under a distant oblique light source. In particular, if the light source is right on top of the surface with $L = (0,0,1)$, the image irradiance equation becomes the Eikonal equation:

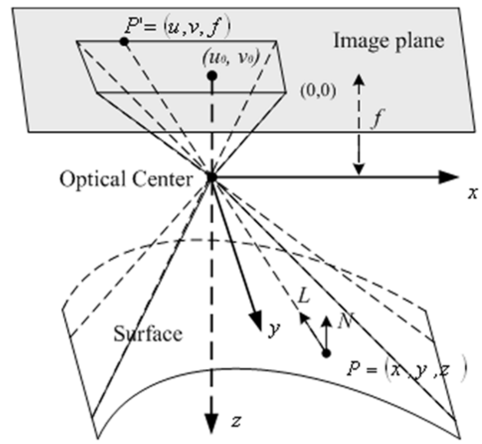

Figure 1. A SFS model with close point light source.

$$\sqrt{p^2+q^2} = \sqrt{1/I(u,v)^2 - 1} \quad (2)$$

However, distant point light source is often difficult to obtain in real-life situations. In fact, it is easier and more practical to capture images using the camera's flash instead of under some specially-built lighting environment. The flash light can be modelled as a close point light source and it is often reasonable to assume that this point light source is located at the optical center because the distance between the camera and the object is usually much greater than the focal length. This gives us the model as shown in Figure 1, where a point $P = (x,y,z)$ on the surface is associated with its image $P' = (u,v,f)$ in the image plane. Subsequently, it is easy to derive that $L = (-x,-y,-z)$ and $N = (p,q,-1)$ at the point P. Given that $x/u = y/v = z/f$, the image irradiance equation becomes:

$$\begin{aligned} I(u,v) &= \frac{(p,q,-1)}{\sqrt{p^2+q^2+1}} \cdot \frac{(-x,-y,-z)}{\sqrt{x^2+y^2+z^2}} \\ &= \frac{-pu-qv+f}{\sqrt{p^2+q^2+1}\sqrt{u^2+v^2+f^2}} \end{aligned} \quad (3)$$

where f is the focal length and (u,v) is the normalized image coordinates with respect to the principle component coordinate (u_0,v_0).

3. Pass I: Lax-Friedrichs Based Sweeping

We observe that the image irradiance equation in Eq. 1 and 3 can be written in the form of a static HJ equation:

$$\begin{cases} H(u,v,\nabla z) = R(u,v), & (u,v) \in \Omega \\ z(u,v) = B(u,v), & (u,v) \in \Gamma \subset \Omega \end{cases} \quad (4)$$

where Ω denotes the image plane, Γ denotes a set of points in Ω at which the value of $z(u,v)$ is known to be $B(u,v)$, called the boundary values, although they may be located in the interior of Ω. In the case of a distant oblique light source as given by Eq. 1, we have:

$$\begin{cases} H(u,v,\nabla z) = I\sqrt{p^2+q^2+1} + p\bar{\alpha} + q\bar{\beta} - \bar{\gamma} \\ R(u,v) = 0 \end{cases} \tag{5}$$

where $(\bar{\alpha}, \bar{\beta}, \bar{\gamma})$ is the normalized illumination direction and $\nabla z = (p,q)$. Similarly, for a close point light source as described by Eq. 3, we have:

$$\begin{cases} H(u,v,\nabla z) & = I\sqrt{p^2+q^2+1}\sqrt{u^2+v^2+f^2} \\ & \quad + pu + qv - f \\ R(u,v) = 0. \end{cases} \tag{6}$$

3.1. Update Based on Lax-Friedrichs Hamiltonian

With the formulation in Eq. 5 and 6, we can then exploit an iterative sweeping strategy [31] to solve for $z(u,v)$ with an update formula based on the Lax-Friedrichs Hamiltonian [15] given as:

$$\begin{aligned} z_{u,v}^{n+1} &= \frac{1}{\frac{\sigma_u}{\Delta u} + \frac{\sigma_v}{\Delta v}} \left(R(u,v) - H(p,q) + \sigma_u u_m + \sigma_v v_m\right) \\ p &= \frac{z_{u+1,v} - z_{u-1,v}}{2\Delta u} \quad q = \frac{z_{u,v+1} - z_{u,v-1}}{2\Delta v} \\ u_m &= \frac{z_{u+1,v} + z_{u-1,v}}{2\Delta u} \quad v_m = \frac{z_{u,v+1} + z_{u,v-1}}{2\Delta v} \end{aligned} \tag{7}$$

where $(\Delta u, \Delta v)$ is the grid size, σ_u and σ_v are artificial viscosities satisfying $\sigma_u \geq \max_{u,v,p,q} |\frac{\partial H}{\partial p}|$ and $\sigma_v \geq \max_{u,v,p,q} |\frac{\partial H}{\partial q}|$. In particular, for Eq. 5, we let

$$\begin{aligned} \sigma_u &= \max_{u,v,p,q} \left|\frac{\partial H}{\partial p}\right| = \max_{u,v}\{\max\{|I+\bar{\alpha}|, |I-\bar{\alpha}|\}\} \\ \sigma_v &= \max_{u,v,p,q} \left|\frac{\partial H}{\partial q}\right| = \max_{u,v}\{\max\{|I+\bar{\beta}|, |I-\bar{\beta}|\}\} \end{aligned} \tag{8}$$

Similarly, for Eq. 6, we let

$$\begin{aligned} \sigma_u &= \max_{u,v,p,q} \left|\frac{\partial H}{\partial p}\right| = \max_{u,v}\{\max\{|I_p+u|, |I_p-u|\}\} \\ \sigma_v &= \max_{u,v,p,q} \left|\frac{\partial H}{\partial q}\right| = \max_{u,v}\{\max\{|I_p+v|, |I_p-v|\}\} \end{aligned} \tag{9}$$

where $I_p = I\sqrt{u^2+v^2+f^2}$.

3.2. Iterative Sweeping Scheme

The iterative sweeping strategy is based on the fast sweeping scheme described by Tsai *et al*. [31]. First, the surface is initialized with the boundary values $B(u,v)$. Next, the value of $z(u,v)$ is updated by sweeping through the image grid in four alternating directions. Finally, after each sweep, the height values are evaluated at the four image boundaries where the update formula fails to compute. The complexity of fast sweeping is $O(N)$ where N is the number of grid points.

4. Pass II: Minimization with Regularization

Essentially, Pass I gives a viscosity solution to the SFS problem. However, it is sensitive to noise. When it applies to real camera images, the noise in the original image or the approximated shading image often cause abrupt errors in the reconstructed result. Nevertheless, if the application is only to restore images with sparse graphical contents to achieve better visual appearance, such a rough estimation might be good enough. However, if we want to improve the OCR performance on those text-dominant images, a better reconstruction is necessary. Therefore, we further apply a least squares method with a regularization term to smooth out the abrupt ridges caused by noises or errors in the approximated shading. Meanwhile, the result in Pass I also provides a good initialization for the minimization method, which avoids the problem of being trapped in local minima.

The minimization method is based on the variational SFS formulation discussed in [13, 8], with the energy:

$$\begin{aligned} F_1(p,q) = & \iint_\Omega [I(p,q) - E(u,v)]^2 \, dudv \\ & + \lambda_i \iint_\Omega \left[\frac{\partial p}{\partial v} - \frac{\partial q}{\partial u}\right]^2 dudv \\ & + \lambda_s \iint_\Omega \left[|\nabla p|^2 + |\nabla q|^2\right] dudv \end{aligned} \tag{10}$$

where p and q are defined same as before, $I(p,q)$ is the image irradiance equation defined in Section 3.1, $E(u,v)$ is the image intensity, λ_i and λ_s are the integrability and smoothing coefficient, respectively. Similarly, in order to derive the height z from p and q, we use the second energy:

$$F_2(z) = \iint_\Omega \left[\left(\frac{\partial z}{\partial u} - p\right)^2 + \left(\frac{\partial z}{\partial v} - q\right)^2\right] dudv \tag{11}$$

To numerically minimize the above two energy functions, we minimize their discrete counterparts. By using forward finite difference approximation to the partial derivatives of p and q, we have the first discrete energy ϵ_1 corresponding to the energy F_1 as follows:

$$\begin{aligned} \epsilon_1(p,q) = & \sum_{(u,v)\in D_\Omega} [I(u,v) - E(u,v)]^2 \\ & + \lambda_i \sum_{(u,v)\in D_\Omega} [(p_{u,v+1} - p_{u,v}) - (q_{u+1,v} - q_{u,v})]^2 \\ & + \lambda_s \sum_{(u,v)\in D_\Omega} [(p_{u+1,v} - p_{u,v})^2 + (p_{u,v+1} - p_{u,v})^2 \\ & \quad + (q_{u+1,v} - q_{u,v})^2 + (q_{u,v+1} - q_{u,v})^2] \end{aligned} \tag{12}$$

where $I(u,v)$ corresponds to Eq. 1 or Eq. 3 under different situations, D_Ω is the discrete domain of Ω. Similarly, the

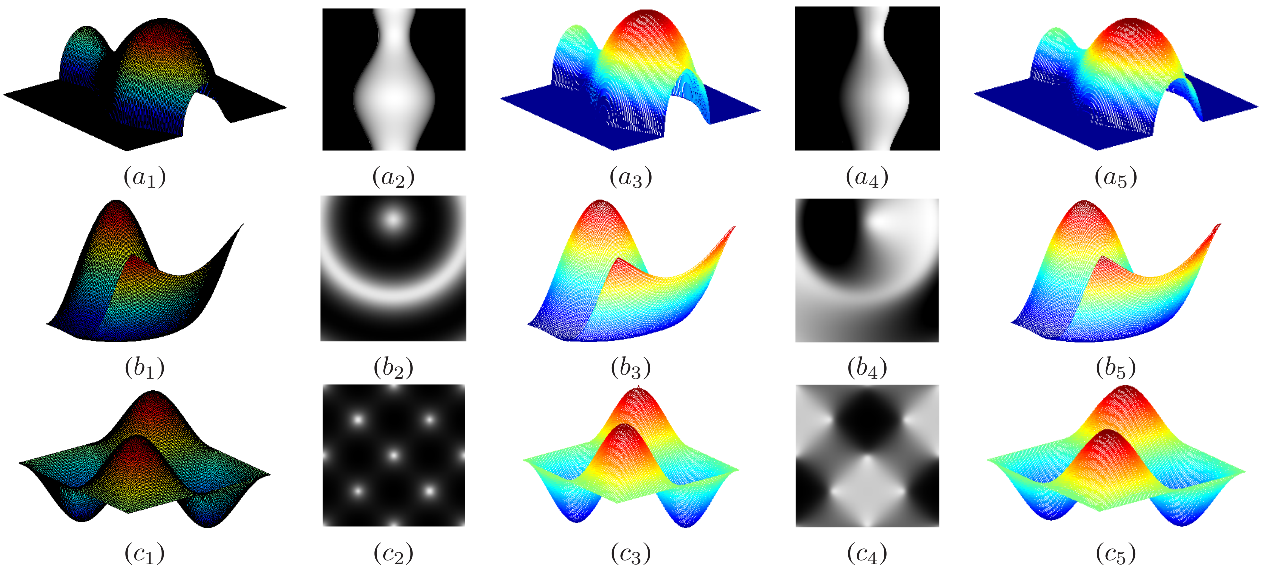

Figure 2. $(a_1)(b_1)(c_1)$ Original surface (ground truth); $(a_2)(b_2)(c_2)$ Shading image with a distant frontal light source $L = (0, 0, 1)$; $(a_3)(b_3)(c_3)$ Reconstructed surface based on Lax-Friedrichs Hamiltonian; $(a_4)(b_4)(c_4)$ Shading image with an oblique light source $L = (1, 0, 1)$; $(a_1)(b_1)(c_1)$ Reconstructed surface based on a high order WENO scheme.

discrete energy ϵ_2 associated with F_2 is:

$$\epsilon_2(z) = \sum_{(u,v)\in D_\Omega} [(z_{u+1,v} - z_{u,v} - p_{u,v})^2 + (z_{u,v+1} - z_{u,v} - q_{u,v})^2] \qquad (13)$$

The energy ϵ_1 and ϵ_2 are minimized by the steepest descent method with a simple line search with Armijo condition [10].

Note that in order to consider all the boundary points, we need to enforce a Neumann boundary condition on p and q. Suppose (m, n) is the size of D_Ω, we then define $p_{0,\cdot} = p_{1,\cdot}$, $p_{m,\cdot} = p_{m+1,\cdot}$, $p_{\cdot,0} = p_{\cdot,1}$ and $p_{\cdot,n} = p_{\cdot,n+1}$. Same applies to q. Given an initialization of (p, q) from Pass I, we first apply an iterative process to find a better configuration $(p, q)_m$ that minimizes ϵ_1 within a certain number of iterations. Next, this new configuration will be used in the evaluation of ϵ_2 in which z is initialized as the result of Pass I. Similar to the previous procedure, we can obtain a new configuration z_m which is the final result.

5. Experimental Results

In our experiments, we first show some results on synthetic surfaces including parametric surfaces and geometric surfaces captured from real 3D object. Comparisons with the original ground truth shape demonstrate our method has robust performance under various lighting situations. On the other hand, due to the many assumptions of the existing SFS methods such as Lambertian reflectance model, constant albedo, and distant point light source, etc, it has always been difficult to apply these methods to real images. Nevertheless, here we show how our 2-pass approach can handle real images better by using examples of real warped document surfaces.

5.1. Results on Synthetic Surfaces

In this experiment, we use three synthetic shading images generated from known parametric surfaces. First, the synthetic vase is generated using the formula provided in [33] as shown in Figure 2 (a_1). The grid size is set to be $\Delta x = \Delta y = 0.00625$ with an image of size 161×161. The second shape is given by Tankus [27]: $z(x, y) = 2cos(\sqrt{x^2 + (y-2)^2} + 100$ as shown in Figure 2 (b_1). The third shape is obtained from [34]: $f(x, y) = 2\pi\sqrt{[cos(2\pi x)sin(2\pi y)]^2 + [sin(2\pi x)cos(2\pi y)]^2}$ as shown in Figure 2 (c_1). The shading images are generated based on Eq. 2 and 1under a distant frontal light source $L = (0, 0, 1)$ and an oblique light source $L = (1, 0, 1)$ as shown in the second and fourth column of Figure 2, respectively. In addition, p and q are discretized using the forward difference of the surface height z.

In the case of a distant frontal light source, we use the formulation described in Eq. 5 with $(\alpha, \beta, \gamma) = (0, 0, 1)$. By applying the iterative sweeping scheme based on Lax-Friedrichs Hamiltonian, we obtain the reconstructed surface as shown in the third column of Figure 2. In particular, the vase surface is initialized with $z = 0$ along the two vertical boundaries. The second shape is initialized with its four boundary values. The last shape is initialized with the five singular points at $(0.25, 0.25), (0.75, 0.75), (0.25, 0.75), (0.75, 0.25)$ and $(0.5, 0.5)$. As we can see that the results are close resem-

Table 1. Evaluation of the efficiency on the three synthetic surfaces.

Surfaces	First order Lax-Friedrichs scheme				High order scheme	
	Frontal light source		Oblique light source		Oblique light source	
	Iteration no.	Total time (s)	Iteration no.	Total time (s)	Iteration no.	Total time (s)
Figure 2(a_1)	17	3.6007	77	19.7733	81	27.6636
Figure 2(b_1)	45	5.0929	93	16.3444	192	39.3084
Figure 2(c_1)	26	5.1727	177	50.9447	195	73.7268

blances of their original surfaces. In addition, we also tried to apply a high order WENO scheme [34] in the case of an oblique light source. More accurate results are obtained as shown in the fifth column of Figure 2. The number of iterations and the total time taken to converge to the solution are given in Table. 1. The convergence criterion used in our experiments is $\max_{u,v} |z^{n+1}_{u,v} - z^{n}_{u,v}| \leq 0.01$.

5.2. Comparisons Using Mozart Bust

To compare our results with those of existing approaches, we use the classic example of Mozart Bust provided by Tsai [33]. The true depth map is captured using a range scanner as shown in Figure 3 (a). Using the same shading generation method described in Section 5.1, we obtain the shading image under an oblique light source ($L = (1, 0, 1)$) as shown in Figure 3 (b). Figure 3 gives the reconstructed shape based on the HJ equation solver discussed in Pass I with an initialization of the singular point on the nose tip. To evaluate the accuracy of the reconstructed shape, we measure its absolute distance from the original true depth map. Figure 4 shows the distance color map. Most of the regions are shown to be well aligned with an average distance of 1.18 mm. In addition, we compare our method with all the algorithms reported in [33]. In particular, Figure 3 (d) shows the result produced by the linear approximation method [30] using the same truth depth map. We can see that the current method gives a much better reconstruction.

5.3. Results on Real Document Images

One of the applications of the SFS technique is in the area of DIR [22, 21, 7]. It can be used to reconstruct the surface shape of a warped document and thus provides a priori knowledge to the restoration process including the removal of both geometric and photometric distortions. Figure 5 shows a general framework of the whole restoration process. One important feature that makes document images different from other images such as facial images or endoscopic images is that document surface's albedo is not constant. Therefore, in order to make the assumption of constant albedo, we need to first extract the intrinsic shading image. This is done using a harmonic inpainting technique [5] followed by a least squares fitting (LSF) with radial basis functions [4]. The inpainting technique essentially re-

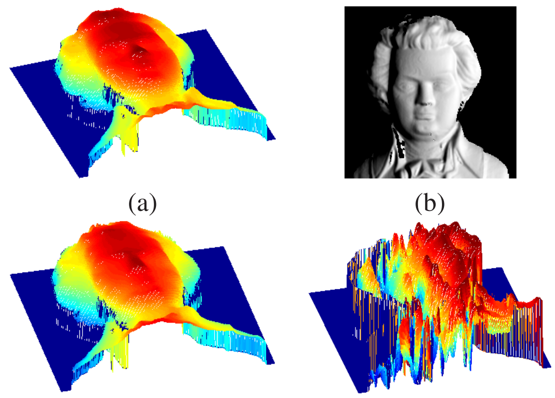

Figure 3. (a) Original depth map of Mozart Bust; (b) Shading image generated with $L = (1, 0, 1)$; (c) Shape reconstructed using the method discussed in Pass I; (d) Shape reconstructed using a linear approximation method.

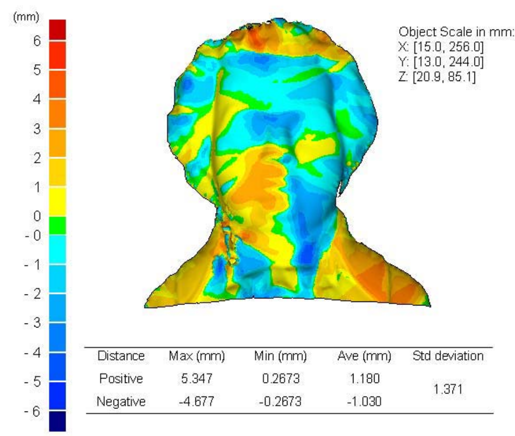

Figure 4. Distance color map of the reconstructed Mozart surface against the original depth map.

moves the texts and graphics from the background. This need not be perfect because the LSF process is insensitive to pixel noise. Once the shading image is extracted, we can derive the photometrically restored image I_p easily based on the notion of intrinsic images [1] which defines each intensity image as composed of two intrinsic images - a shading image and a reflectance image. Typically, for Lambertian surfaces, the intensity image is the product of the two components [29]. Therefore, the reflectance image is easily obtained as: $I_r = e^{log\, I - log\, I_s}$. The photometrically re-

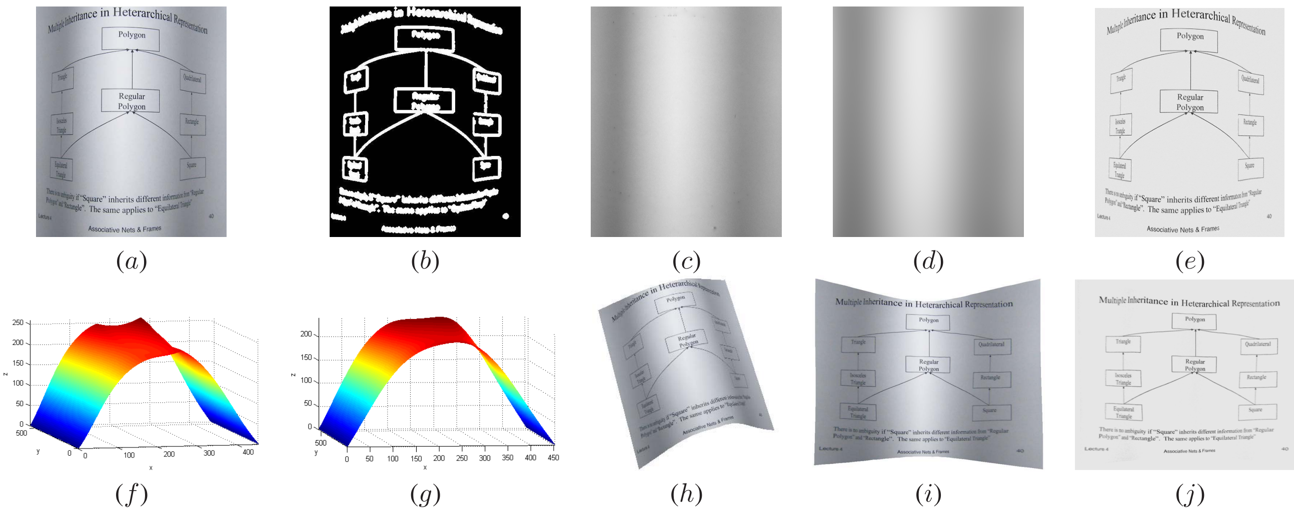

Figure 6. (a) Original warped image (cropped from an image of size 1600×1200); (b) Inpainting mask; (c) Inpainted image; (d) Extracted shading image; (e) Photometrically restored image with $k = 0.9$; (f) Reconstructed shape after pass I; (g) Reconstructed shape after pass II; (h) Original warped image mapped onto the surface mesh; (i) Geometrically restored image; (j) Final restored image.

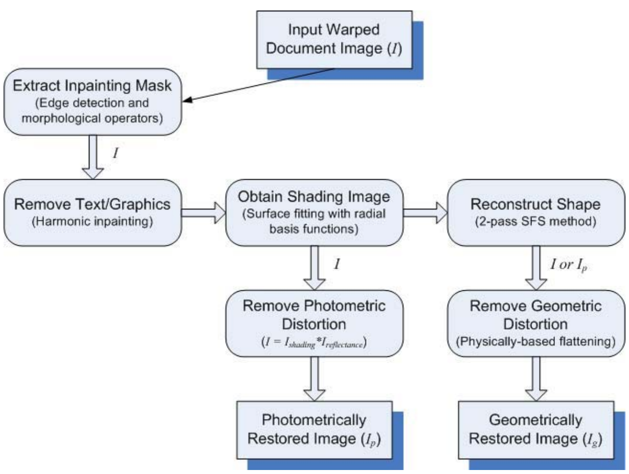

Figure 5. A general framework of the DIR process.

stored image can thus be computed as: $I_p = k \cdot I_r$, where $k \in [0, 1]$. On the other hand, the extracted shading image can also be used to reconstruct the surface shape through the 2-pass SFS method as discussed earlier. The surface shape describes how the document is warped and it can be forced to a plane through a physically-based flattening process [2, 6]. Meanwhile, the original document image is mapped to the reconstructed shape based on $x/u = y/v = z/f$ so that it is restored to its planar form accordingly when the shape is flattened. Finally, the restored image I_g is obtained with the geometric distortions removed. Similarly, by using I_p as the texture of the warped surface, we get the image with both geometric and photometric distortions removed.

In our experiments, all the warped images are taken in a relatively dark environment with the camera's flash simulating a close point light source. In addition, the camera's focal length and principle components are obtained through a simple calibration procedure. Typically, for an image of size 1600×1200, we have $f = 1348.28$ and $(u_0, v_0) = (790.24, 581.85)$ in pixel size. The images are cropped to avoid lens distortions near the corners. Moreover, gamma correction is performed by applying an inverse power function $1/gamma$ to the RGB values, since most of cameras are calibrated to compensate for the display device with a gamma value.

Figure 6 shows an example of an arbitrarily curved document with mixed figures and texts. From Figure 6 (d) and (e), we can see that the extracted shading image reflects the illumination change nicely and is separated well from the reflectance image. A good shading image definitely accounts for a more accurate reconstruction since shading is the sole information used as the SFS input. Next, Figure 6 (f) and (g) demonstrate how the minimization procedure improves the reconstructed shape through the second pass. The first pass is initialized by setting the height at the two vertical boundaries to 0. This could be any arbitrary value because the reconstructed shape is invariant up to a translation factor. Figure 6 (h) shows the reconstructed shape with the original warped image mapped as the texture. Finally, Figure 6 (i) and (j) give the restored images. It is noticed that the restored image is much better improved comparing to the original image although there are still some distortions due to the imperfection of the estimated shape.

Figure 7 shows another example of a diagonally curved document with mainly text contents. This randomly curved document does not have obvious boundaries lie on the same plane. In this case, we use the singular points as the initialization condition in the first pass. Experiments show that even if the singular points are slightly off, the result is not

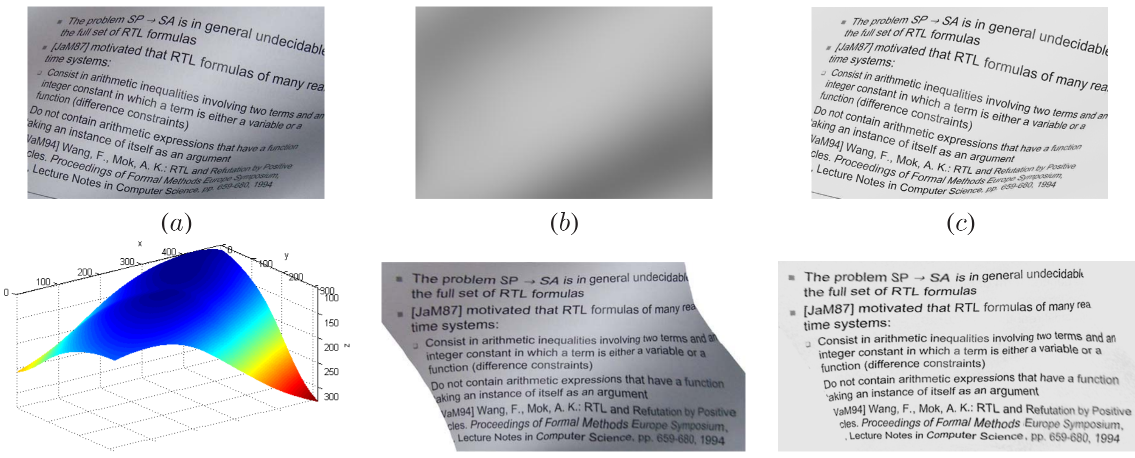

Figure 7. (a) Original warped image; (b) Extracted shading image; (c) Photometrically restored image with $k = 0.9$; (d) Reconstructed shape by initializing singular points; (e) Geometrically restored image; (f) Final restored image.

affected much. Figure 7 (d) and (e) show the reconstructed shape and the geometrically restored image, respectively. We can see that the shape does emulate the original curvature though it is not a perfect reconstruction. The restored image also shows a better visual appearance despite some unremoved distortions. In terms of OCR performance, the restored image gives a word precision of 95.6% comparing to 38.9% on the original image. Moreover, we have collected a total of 20 warped document images with approximately 2,400 words for OCR testing. The average word precision is 94.3% on the restored images in contrast to 43.6% on the original images.

5.4. Discussion

Our results on synthetic surfaces have shown that the sweeping method based on Lax-Friedrichs Hamiltonian can produce good results on perfect shading images with accurate initialization conditions. However, in the real situation, shadings are often imperfect due to several hard-to-control factors such as lighting, surface material, lens distortion, etc. The use of Pass II to further improve the first-step reconstruction is thus necessary to produce a better reconstruction for subsequent restoration processes.

The successful application of SFS technique to DIR provides solutions to several problems that traditional 2D DIR methods cannot handle. In particular, for the image in Figure 6, those textline-based DIR methods [35] will fail because of the lack of textlines. Moreover, the current SFS-based approach does not restrict to cylindrical surfaces as opposed to some existing 3D modeling methods [3]. In addition, comparing to methods that use stereo-based shape recovery technique [2], the current method gives a good start in terms of working around a single image. More importantly, the shading extraction procedure itself provides crucial information to the separation of reflectance image, which naturally leads to the photometrically restored image. However, the proposed SFS method currently only deals with smoothly curved documents but not folds as discussed in [26], so sharp edges are often smoothed out at the ridges. Further studies will be extended in this direction.

6. Conclusion

In this paper, we proposed a 2-pass SFS method under different lighting conditions and discussed its applications in the area of document image restoration. In Pass I, we expressed the image irradiance equation under both distant and close point light sources to a form of the HJ equation, which is then solved using a sweeping method based on Lax-Friedrichs Hamiltonian. Experiments on synthetic surfaces showed that this method gives good reconstruction results based on perfect shading images and could be further improved with a high order WENO scheme. Moreover, the minimization method in Pass II starts with a good estimation returned from Pass I and further improves the shape with a regularization technique. This method is less sensitive to noise and thus produces better results on real images. Experiments on real document images also provide evidence for this. In addition, we also developed a general framework for restoring document images with both geometric and photometric distortions using the SFS technique. Each of the preprocessing steps for extracting the shading image is crucial for a good reconstructed shape. Currently, we are assuming that the camera's flash is close to the optical center in real applications. This can be further relaxed by incorporating the light source location into the SFS formulation. We are looking into this direction and hoping that better results can be achieved in the future.

7. Acknowledgment

This research is supported in part by National University of Singapore URC grant R252-000-202-112 and Agency for Science, Technology and Research(A*STAR) grant 0421010085.

References

[1] H. Barrow and J. Tenenbaum. *Recovering Intrinsic Scene Characteristics from Images*. Academic Press, 1978. 5

[2] M. Brown and W. Seales. Image restoration of arbitrarily warped documents. *IEEE Trans. on Pattern Analysis and Machine Intelligence*, 26(10):1295–1306, 2004. 6, 7

[3] H. Cao, X. Ding, and C. Liu. A cylindrical model to rectify the bound document image. *Int'l Conf. on Computer Vision*, 2:228–233, 2003. 7

[4] J. Carr, R. Beatson, J. Cherrie, T. Mitchell, W. Fright, B. McCallum, and T. Evans. Reconstruction and representation of 3d objects with radial basis functions. *ACM SIGGRAPH 2001*, pages 67–76, 2001. 5

[5] T. Chan and J. Shen. Mathematical models for local nontexture inpaintings. *SIAM Journal on Applied Mathematics*, 62(3):1019–1043, 2002. 5

[6] K. Chua, L. Zhang, Y. Zhang, and C. Tan. A fast and stable approach for restoration of warped document images. *ICDAR'05*, pages 384–388, 2005. 6

[7] F. Courteille, A. Crouzil, J. Durou, and P. Gurdjos. A unifying and rigorous shape from shading method adapted to realistic data and applications. *Int'l Conf. on Pattern Recognition*, 2:277–280, 2004. 2, 5

[8] A. Crouzil, X. Descombes, and J. Durou. A multiresolution approach for shape from shading coupling deterministic and stochastic optimization. *IEEE Trans. on Pattern Analysis and Machine Intelligence*, 25(11):1416–1421, 2003. 3

[9] J. Durou, M. Falcone, and M. Sagona. A survey of numerical methods for shape from shading, 2004. Research Report from IRIT. 2

[10] R. Fletcher. *Practical Methods of Optimization*. John Wiley and Sons, New York, 2nd edition, 1987. 4

[11] R. Frankot and R. Chellappa. A method for enforcing integrability in shape from shading algorithms. *IEEE Trans. on PAMI*, 10:439–451, 1988. 1

[12] B. Horn. Obtaining shape from shading information. In *The Psychology of Computer Vision (P.H. Winston)*, New York, 1975. McGraw-Hill. 1

[13] B. Horn and M. Brooks. The variational approach to shape from shading. *Computer Vision, Graphics, and Image Processing*, 33(2):174–208, 1986. 1, 3

[14] K. Ikeuchi and B. Horn. Numerical shape from shading and occluding boundaries. *AI*, 17(1):141–184, 1981. 1

[15] C. Kao, S. Osher, and J. Qian. Lax-friedrichs sweeping scheme for static hamilton-jacobi equations. *Journal of Computational Physics*, 196(1):367–391, 2004. 3

[16] R. Kimmel and A. Bruckstein. Tracking level sets by level sets: A method for solving the shape from shading problem. *Computer Vision, Graphics, Image Processing: Image Understanding*, 62(2):47–58, 1995. 1

[17] R. Kimmel and J. Sethian. Optimal algorithm for shape from shading and path planning. *Journal of Mathematical Imaging and Vision*, 14(2):237–244, 2001. 1

[18] J. Oliensis and P. Dupuis. Direct method for reconstructing shape from shading. *SPIE*, pages 116–128, 1991. 1

[19] S. Osher and J. Sethian. Fronts propagating with curvature dependent speed:algorithms based on the hamilton-jacobi formulation. *Journal of Computational Physics*, 79:12–49, 1988. 1

[20] A. Pentland. Local shading analysis. *IEEE Trans. on Pattern Analysis and Machine Intelligence*, 6:170–187, 1984. 2

[21] E. Prados, F. Camilli, and O. Faugeras. A unifying and rigorous shape from shading method adapted to realistic data and applications. *Journal of Mathematical Imaging and Vision*, 25(3):307–328, 2006. 1, 5

[22] E. Prados and O. Faugeras. A rigorous and realistic shape from shading method and some of its applications, 2004. Research Report from INRIA. 1, 2, 5

[23] E. Prados and S. Soatto. Fast marching method for generic shape from shading. *VLSM'05*, page 320C331, 2005. 1

[24] E. Rouy and A. Tourin. A viscosity soluition approach to shape from shading. *SIAM Journal on Numerical Analysis*, 3(29):867–884, 1992. 1

[25] J. Sethian. *Level Set Methods and Fast Marching Methods*. Cambridge University Press, New York, 1999. 1

[26] M. Sun, R. Yang, L. Yun, G. Landon, B. Seales, and M. Brown. Geometric and photometric restoration of distorted documents. *IEEE Int'l Conf. on Computer Vision*, 2:17–21, 2005. 7

[27] A. Tankus, N. Sochen, and Y. Yeshurun. A new perspective on shape-from-shading. *IEEE International Conference on Computer Vision*, 2:862–869, 2003. 4

[28] A. Tankus, N. Sochen, and Y. Yeshurun. Perspective shape-from-shading by fast marching. *Int. Conf. on Computer Vision and Pattern Recognition*, 1:43–49, 2004. 1

[29] M. Tappen, W. Freeman, and E. Adelson. Recovering intrinsic images from a single image. *IEEE trans. on PAMI*, 27(9):1459–1472, 2005. 5

[30] P. Tsai and M. Shah. Shape from shading using linear approximation. *Journal of Image and Vision Computing*, 12(8):487–498, 1994. 1, 5

[31] Y. Tsai, L. Cheng, S. Osher, and H. Zhao. Fast sweeping algorithms for a class of hamilton-jacobi equations. *SIAM Journal on Numerical Analysis*, 41(2):659–672, 2003. 1, 3

[32] S. Yuen, Y. Tsui, Y. Leung, and R. Chen. Fast marching method for shape from shading under perspective projection. *Visualization, Imaging, and Image Processing*, pages 584–589, 2002. 1

[33] R. Zhang, P. Tsai, J. Cryer, and M. Shah. Shape from shading: A survey. *IEEE Trans. on Pattern Analysis and Machine Intelligence*, 21(8):690–706, 1999. 2, 4, 5

[34] Y. Zhang, H. Zhao, and J. Qian. High order fast sweeping methods for eikonal equations. *Proc. of the 74th SEG Annual International Meeting*, pages 1901–1904, 2004. 4, 5

[35] Z. Zhang and C. Tan. Correcting document image warping based on regression of curved text lines. *Int'l Conf. on Document Analysis and Recognition*, pages 589–593, 2003. 7